Progress In Electromagnetics Research, PIER 68, 71–90, 2007

ANALYSIS OF INDUCTIVE WAVEGUIDE MICROWAVE COMPONENTS USING AN ALTERNATIVE PORT TREATMENT AND EFFICIENT FAST MULTIPOLE

F. J. P. Soler, F. D. Q. Pereira, J. P. García, D. C. Rebenaque and A. Á. Melcón

Technical University of Cartagena
Antiguo Cuartel de Antigones, s/n, E-30202 Cartagena, Spain

Abstract—This paper presents a simple and alternative approach for the analysis of inductive waveguide microwave components. The technique uses a surface integral equation formulation, in which the contours of the waveguide walls and of the inner obstacles are all discretized using triangular basis functions. In order to avoid the relative convergence problem of other techniques based on mode matching, an alternative port treatment is used. The technique is based on the application of the extinction theorem using the spatial representation of the Green's functions in the terminal waveguides. In addition, the Fast Multipole Method is proposed in order to reduce the computational cost for large problems. Different complex structures are analyzed, including microwave bandpass filters with elliptic transfer functions, waveguide bends and T-junctions. Results show the high accuracy and versatility of the technique derived.

1. INTRODUCTION

The study of waveguide inductive structures, due to its practical interest in many microwave applications, has been reflected in an important number of technical papers during the last decades [1]. For the analysis of this type of structures, several approaches were derived in the past, including the finite elements method [1] and techniques based on modal analysis [2, 3]. The techniques based on modal analysis expand the electromagnetic fields as a series of modes inside the waveguide, and then the boundary conditions for the fields are imposed at junctions and discontinuities. The form in which these boundary conditions are enforced leads either to mode matching [2] or to integral equation formulations [3], including multimode network

approaches [4]. In general, methods based on modal analysis are very efficient, but they are limited to simple or canonical geometries, where the modes can be calculated analytically [4].

In addition, modal analysis can be combined with integral equation formulations, if the spectral representation of the Green's functions inside a parallel plate waveguide is used [5]. An important limitation of this technique is that all obstacles or coupling windows must be placed inside the parallel plate waveguide considered. Also the input and output ports must be lined-up, sharing the based parallel plate waveguide. This limits the possibility to analyze other useful waveguide components such as bends, filters with elliptic responses [6] or T-junctions.

To overcome these difficulties, other authors have used integral equations formulations based on the free space Green's functions. In this case the contour of the base waveguide needs to be discretized, in addition to the inductive posts and windows. The difficulty in this approach is how to model the ports exciting the structure. In [7–9], this problem was solved by applying a mode matching procedure between the waveguide ports and the internal circuit structure. While these approaches are valid, it is well known that care must be taken to avoid relative convergence problems. On the other hand, these approaches open the possibility for the analysis of the more complex microwave devices mentioned above (see Fig. 1).

In this work we present an integral equation technique based on the free space Green's functions, with an alternative port treatment. The extinction theorem is used to separate the internal finite circuit structure from the access ports. Two ground planes are placed at the reference port positions, and are connected through the external problem to infinite waveguide sections. The technique uses the Green's functions with respect to one port-ground plane (the excitation port), to model the internal finite circuit problem. The Green's functions in this case are easily formulated using the classical image theory. On the other hand, for the external port problem a spatial representation of the parallel plate Green's functions is used to model the semi-infinite port waveguides. The spatial representation of the Green's functions is very convenient in this case, since complex basis functions can be used in the discretization of the ports. The spatial representation of the Green's functions that we have used is based on the convergence acceleration technique of series presented in [10]. Other approaches based on spectral representations need specific type of basis functions [11], therefore losing the flexibility of the technique proposed in this contribution.

Another contribution of this paper is the application of the Fast

Multipole Method (FMM) to the analysis of waveguides components using the above IE strategy. It is known that the FMM can be used to reduce the computational cost for large problems. In the past it has been employed to solve large scattering problems [12, 13]. In this work we apply for the first time the FMM to the analysis of inductive waveguide components, where the near field must accurately be obtained in order to recover the electrical behavior of the device.

Results for several useful microwave circuits employing both direct and FMM approaches will be presented, showing the high accuracy and flexibility of the alternative technique developed in this paper.

2. THEORETICAL OUTLINE

The analysis of a general inductive waveguide multiport structure shown in Fig. 1 is analyzed using an integral equation formulation. The technique is based on the evaluation of the admittance parameters (Y) of the multiport structure. This is done by alternatively considering an incoming excitation wave on each port (j), and short-circuiting all others (i). For each case the electric and magnetic fields on the ports have to be evaluated. Then, the final Y-parameters are

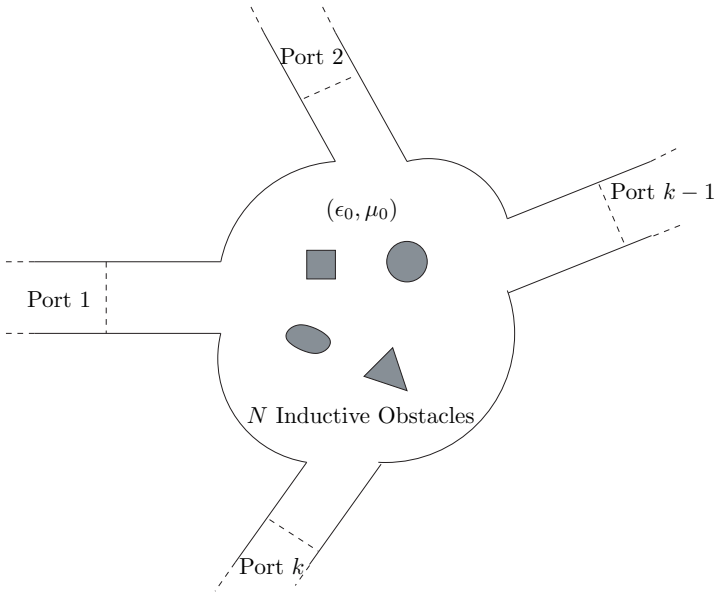

Figure 1. Typical multiport inductive waveguide problem studied in this paper, containing N metallic obstacles.

computed through integration of the fields with the corresponding modal functions:

$$Y_{m,n}^{(i,j)} = \frac{\iint_{S_i} \vec{H}_t^{(i)} \cdot \vec{h}_m^{(i)} dS}{\iint_{S_j} \vec{E}_t^{(j)} \cdot \vec{e}_n^{(j)} dS} \tag{1}$$

For the computation of the fields an integral equation is formulated. The integral equation is applied to arbitrarily shaped inductive structures, by discretizing the contour of the base waveguide and of the inner obstacles (see Fig. 1), using triangular roof-top type functions defined on linear segments. The excitation input port is isolated from this analysis using the extinction theorem. The original problem is divided in the two classical internal and external problems. The internal circuit problem is discretized using the above defined mesh, placing in addition equivalent magnetic current densities at the port position ($-\vec{M}$). A ground plane is placed at the reference plane to short-circuit any electric currents, as shown in Fig. 2.

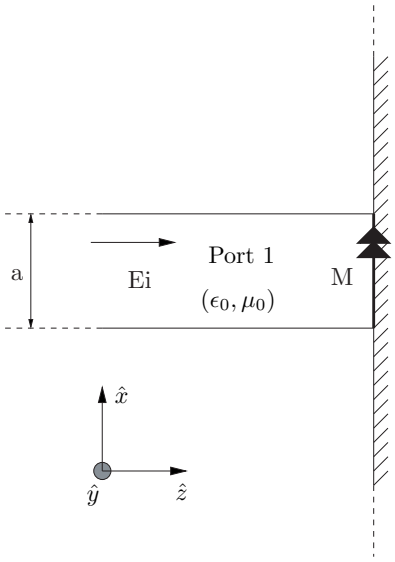

Figure 2. Internal circuit problem resulting from the application of the extinction theorem.

For the solution of this problem the Green's functions to be used are those in the presence of an infinite ground plane. The Green's functions can therefore be easily formulated using image theory [14].

In Section 2.1 a procedure is outlined for the calculation of the Green's functions in the presence of an arbitrarily oriented ground plane. This has proved useful in the analysis of inductive bends and Y-junctions, when one port can be placed at reference axis with different slopes.

On the other hand, the external port problem assumes an incoming wave in a semi-infinite waveguide as shown in Fig. 3. The

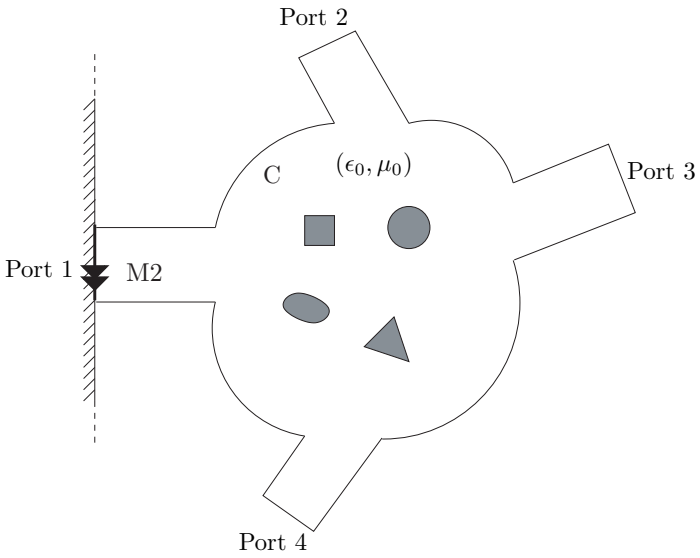

Figure 3. External port problem resulting from the application of the extinction theorem.

coupling to the internal problem is accomplished by placing equivalent magnetic currents at the reference plane. In this case, a magnetic current density equal to $(2\,\bar{M})$ is assumed in order to eliminate the ground plane. The resulting problem is, therefore, reduced to the evaluation of the Green's functions for magnetic currents inside an infinite parallel plate waveguide. The main difficulty for the evaluation of these Green's functions is that they are formulated either as modal series or as spatial images series, both exhibiting very slow convergence behaviors. Some approaches in the past have used spectral representations of the series with a particular choice of the basis functions to accelerate convergence [11]. Instead, in this work we have preferred to obtain a representation of the Green's functions directly in the spatial domain. We have done this by using the series acceleration techniques presented in [10], together with a proper combination of the spectral and spatial formulations of the series [15]. The advantage of

having the Green's functions in the spatial domain, is that the same discretization scheme used for the internal circuit problem can also be used in the characterization of the ports. This strategy has shown to increase the flexibility of the technique, allowing for the analysis of complex inductive waveguide devices without loosing accuracy or efficiency. In addition, the relative convergence problem of other mode matching techniques [7, 8] is avoided with the proposed technique.

After imposition of the boundary conditions for the fields in the structure, the following coupled integral equations are obtained:

$$\begin{aligned}\hat{n}\times\vec{H}^{(exc)} \;=\; \hat{n}\times\Bigg\{ & j\,\omega\left[2\,\overline{\overline{G}}_F^{(ext)}+\overline{\overline{G}}_F^{(int)}\right]\otimes\vec{M} \\ & -\frac{1}{j\,\omega}\,\nabla\left[\left(2\,G_W^{(ext)}+G_W^{(int)}\right)\otimes\left(\nabla'\cdot\vec{M}\right)\right] \\ & +\frac{1}{\mu_0}\,\nabla\times\left[\overline{\overline{G}}_A^{(int)}\otimes\vec{J}_c\right]\Bigg\}; \qquad \text{at port on } s_m \end{aligned} \tag{2a}$$

$$0 \;=\; \hat{n}\times\left\{\frac{1}{\epsilon_0}\,\nabla\times\left[\overline{\overline{G}}_F^{(int)}\otimes\vec{M}\right]-j\omega\left(\overline{\overline{G}}_A^{(int)}\otimes\vec{J}_c\right)\right\};\ \text{on } s_e \tag{2b}$$

where superscript (ext) is used to denote the Green's functions of the external problem, and (int) denotes the Green's functions of the internal problem. Moreover, $\vec{H}^{(exc)}$ is the magnetic field of the $TE_{1,0}$ mode in the excitation waveguide, and $\otimes$ denotes a convolution (superposition) integral. Also, note that for the inductive waveguide problems treated in this work there are no contributions from the electric scalar potential. This is because its gradient is orthogonal to the induced electric currents in the metallic areas of the structure.

2.1. Green's Functions in the Presence of Arbitrarily Oriented Ground Plane

As already discussed, the integral equation solution of the internal circuit problem involves the two dimensional Green's functions in the presence of an infinite ground plane with arbitrary orientation. This is specially useful in the analysis of inductive bends and Y-junctions, where the axis ports can have different slopes. In this section a simple geometrical procedure to determine the Green's functions in this situation is presented.

For a unitary current of magnetic type, the geometrical image problem is shown in Fig. 4. The direction of the image dipole can be

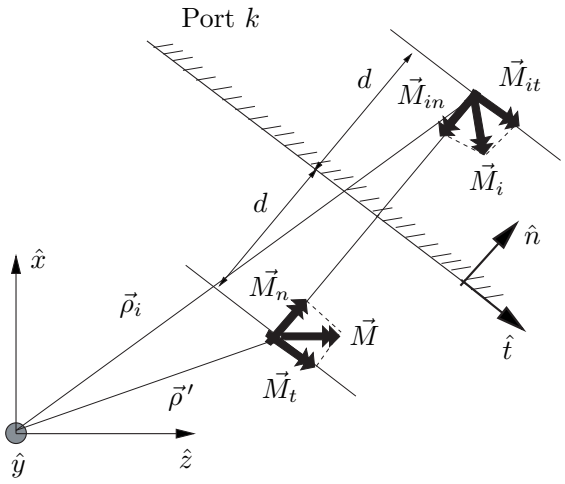

Figure 4. Source and image magnetic dipoles for an arbitrarily oriented ground plane.

found by first casting the source dipole into two components. One is oriented along the unitary vector tangential to the ground plane ($\hat{t}$), while the other along the normal direction to the plane ($\hat{n}$). Following this decomposition, the relevant components of the dyadic magnetic and electric vector potentials Green's functions take the following form:

$$G_A^{yy}(\vec{\rho},\vec{\rho}') = \frac{\mu_0}{4j}\left[H_0^{(2)}(k_0|\vec{\rho}-\vec{\rho}'|) - H_0^{(2)}(k_0|\vec{\rho}-\vec{\rho}_i|)\right] \tag{3a}$$

$$G_F^{xx}(\vec{\rho},\vec{\rho}') = \frac{\epsilon_0}{4j}\Bigg\{H_0^{(2)}(k_0|\vec{\rho}-\vec{\rho}'|) + \Big[H_0^{(2)}(k_0|\vec{\rho}-\vec{\rho}_i|)\,(\hat{t}\cdot\hat{x})\,\hat{t} - H_0^{(2)}(k_0|\vec{\rho}-\vec{\rho}_i|)\,(\hat{n}\cdot\hat{x})\,\hat{n}\Big]\cdot\hat{x}\Bigg\} \tag{3b}$$

$$G_F^{zz}(\vec{\rho},\vec{\rho}') = \frac{\epsilon_0}{4j}\Bigg\{H_0^{(2)}(k_0|\vec{\rho}-\vec{\rho}'|) + \Big[H_0^{(2)}(k_0|\vec{\rho}-\vec{\rho}_i|)\,(\hat{t}\cdot\hat{z})\,\hat{t} - H_0^{(2)}(k_0|\vec{\rho}-\vec{\rho}_i|)\,(\hat{n}\cdot\hat{z})\,\hat{n}\Big]\cdot\hat{z}\Bigg\} \tag{3c}$$

where only simple vector operations involving the tangent and normal unitary vectors are needed. The position of the image dipole is found to be: $\vec{\rho}_i = \vec{\rho}' + 2\,d\,\hat{n}$.

It is important to note that, if the excitation port is slanted with respect to the vertical axis, then cross components for the vector potentials are generated by the image dipole. Using the same geometrical considerations as before, we easily find the cross components as:

$$G_F^{xz}(\vec{\rho},\vec{\rho}\,') = G_F^{zx}(\vec{\rho},\vec{\rho}\,') = \frac{\epsilon_0}{4j}\left\{\left[H_0^{(2)}(k_0|\vec{\rho}-\vec{\rho}_i|)(\hat{t}\cdot\hat{x})\hat{t} - H_0^{(2)}(k_0|\vec{\rho}-\vec{\rho}_i|)(\hat{n}\cdot\hat{x})\hat{n}\right]\cdot\hat{z}\right\} \tag{4}$$

Similar calculations can be done with point charges for the magnetic scalar potential Green's functions, obtaining:

$$G_W(\vec{\rho},\vec{\rho}\,') = \frac{1}{4\,j\,\mu_0}\left[H_0^{(2)}(k_0|\vec{\rho}-\vec{\rho}\,'|) + H_0^{(2)}(k_0|\vec{\rho}-\vec{\rho}_i|)\right] \tag{5}$$

Since the electric scalar potential does not contribute to inductive structures, this last step completes the formulation of all the Green's functions components of the internal problem, needed in our formulation. These Green's functions are used for the internal problem, and are coupled to those derived in [10] for the external problem (waveguide port).

3. APPLICATION OF THE FAST MULTIPOLE METHOD

The image theory used to formulate the Green's functions for the internal problem, splits each interaction into two free-space based Green's functions [16]. Due to this fact, the Fast Multipole Method (FMM) acceleration technique [17], can be applied for solving the internal problem of the previous section. FMM allows a decomposition of the free space Green's function and its derivatives, which reduces the computational cost for big problems, saving at the same time memory requirements. The method has been applied in the past to the analysis of large scattering problems in two and three dimensions [18, 12], but here we show a new application of the technique with the analysis of inductive waveguide components.

The main new features that differ from other applications of the FMM are the treatment of the interactions of the spatial images, and also the usage of triangular basis functions instead of the classical Point Matching approach, as applied to two-dimensional problems. For previous scattering applications the important quantity was the far-field scattered by the large object. For this new application accuracy

must also be preserved during the calculation of the near field. This is of primary importance, since the electrical behavior of the waveguide device is extracted from this near field, as stated in equation (1).

Another interesting issue concerning the application of the FMM with this formulation is how to treat the external problem. For this external problem the parallel plate Green's functions are computed using the spectral domain series with the technique derived in [10]. Consequently, the FMM cannot be applied directly to this external problem. Instead, the corresponding interactions will be calculated using a direct Method of Moments (MoM) implementation. However, this does not represent a major drawback, since the external problem only contains the unknowns associated to the exciting port, and this represents just a small part of the total amount of unknowns. Once the external problem is computed, it can be easily incorporated to the nearest neighbours matrix, which is one of the components of the FMM technique itself.

3.1. Separation of the Interactions in Two Parts

As shown in (3a), the spatial images technique splits each single interaction into two parts, namely the observation-source point interaction, and the observation-image point interaction. For example, in the case of dyadic component (G_A^{yy}) for two points, from source cell i to observer cell j, we have:

$$G_A^{yy}(\vec{\rho_j}, \vec{\rho_i}) = \frac{\mu_0}{4j}\left[H_0^{(2)}(k_0\,|\vec{\rho_j} - \vec{\rho_i}^{(s_o)}|) - H_0^{(2)}(k_0\,|\vec{\rho_j} - \vec{\rho_i}^{(s_i)}|)\right] \quad (6)$$

where (s_o) denotes the original source and (s_i) the corresponding image source. Moreover, $\vec{\rho_j}$ denotes a point inside the observer cell and $\vec{\rho_i}$ is a point inside the source cell.

Now, let us consider the case of an interaction between elements of two different metallic posts, on which the dyadic component (6) is needed. Using supperposition, the MoM matrix element Z_{ji} can be decomposed into two parts, obtaining:

$$\begin{aligned} Z_{ji} &= j\omega \int_C G_A^{yy}(\vec{\rho_j}, \vec{\rho_i})\; J_z(\vec{\rho_i})\; dc_i \\ &= j\omega \int_C H_0^{(2)}(k_0|\vec{\rho_j} - \vec{\rho_i}^{(s_o)}|)\; J_z(\vec{\rho_i})\; dc_i \\ &\quad -j\omega \int_C H_0^{(2)}(k_0|\vec{\rho_j} - \vec{\rho_i}^{(s_i)}|)\; J_z(\vec{\rho_i})\; dc_i \\ &= Z_{ji}^{(s_o)} + Z_{ji}^{(s_i)} \end{aligned} \quad (7)$$

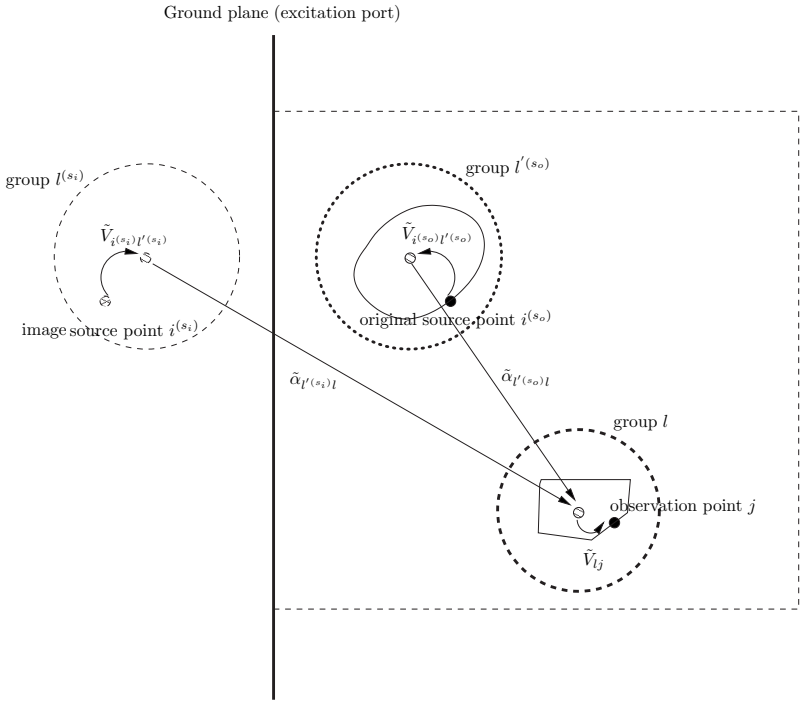

Figure 5. Agregation, translation and disagregation stages for both source and image points in an interaction between two posts.

The key of FMM consists on dividing the spatial geometry of the problem into groups, assigning each discretization (mesh) cell to the closest group. Then, the method applies, for each interaction between a pair of basis and test functions, a decomposition process in three stages. The first one is called *aggregation*, and serves to pass the information from the source point to the center of the corresponding group, by means of the operator $\tilde{V}_{agg}$. The second is the *translation*, and it is used to transfer the information from the center of the source group to the center of the observation group, using the operator $\tilde{\alpha}$. Finally, the third stage is called *disaggregation*, and it is the opposite operation to the aggregation (the operator $\tilde{V}_{dgg}$ recovers the information from the center of the group to the final observation point).

Now, this decomposition can be applied independently to each one of the parts in (7), as shown in Fig. 5. In the case of the image point, as it is located in the opposite side of the ground plane, an imaginary group is needed to evaluate the corresponding aggregation

and translation processes. Since the observation point does not change for the original and for the image sources, the disaggretation operator will be the same in both cases, avoiding new calculations. Applying the decomposition as described above, the expression for the MoM matrix element (7) would turn into:

$$Z_{ij} = \int_0^{2\pi} \tilde{V}_{dgg}(\alpha)\ \tilde{\alpha}_{ll'(s_o)}(\alpha)\ \tilde{V}_{agg}^{(s_o)}(\alpha)\ d\alpha - \int_0^{2\pi} \tilde{V}_{dgg}(\alpha)\ \tilde{\alpha}_{ll'(s_i)}(\alpha)\ \tilde{V}_{agg}^{(s_i)}(\alpha)\ d\alpha \tag{8}$$

where $\tilde{\alpha}_{l'l(\xi)}(\alpha)$ is a diagonalized translator operator [17] between the centers of the observer group (l) and source group ($l^{'(\xi)}$) (in our case for both original and image sources: $\xi = s_o, s_i$). This operator can be written as:

$$\tilde{\alpha}_{ll'(\xi)}(\alpha) = \sum_{p=-P}^{P} H_p^{(2)}(k\rho_{ll'(\xi)})\ e^{jp\ \cos(\alpha - \phi_{ll'(\xi)})} \tag{9}$$

where $\phi_{ll'(\xi)}$ denotes the angle of the spatial vector ($\vec{\rho}_{ll'(\xi)}$) with respect to the origin, and P is a truncation parameter which controls the accuracy of the approximation of the Hankel function's actual value.

The aggregation and disaggretation operators have the following general expression:

$$\tilde{V}_{agg}^{(\xi)}(\alpha) = \int_C \beta_{i(\xi)l}(\alpha)\ \vec{f}_b(\vec{\rho}_i^{(\xi)}) \cdot \hat{y}\ dc_i; \qquad \xi = s_o, s_i \tag{10a}$$

$$\tilde{V}_{dgg}(\alpha) = \int_C \beta_{l'j}(\alpha)\ \vec{f}_t(\vec{\rho}_j) \cdot \hat{y}\ dc_j \tag{10b}$$

with:

$$\beta_{i(\xi)l'(\xi)}(\alpha) = C_{agg}\ e^{-jk\rho_{i(\xi)l'(\xi)}\ \cos(\alpha - \phi_{i(\xi)l'(\xi)})} \tag{11a}$$

$$\beta_{lj}(\alpha) = C_{dgg}\ e^{-jk\rho_{lj}\cos(\alpha - \phi_{lj})} \tag{11b}$$

In equation (11a), $\vec{f}_t$, $\vec{f}_b$ are the test and basis functions respectively, and C_{agg}, C_{dgg} are expressions that depend on the kind of interaction computed (generated either by an electric or by a magnetic current source). For example, for an interaction between two metallic posts (electric-electric interaction) we have $C_{agg} = 1$ and $C_{dgg} = \omega\mu/4Q$, being Q the number of quadrature points employed in the integral along the group circumference.

If we use this formulation combined with a Point Matching formulation of the MoM (employing delta functions for test and pulse as basis functions), the original expressions in (10a) turn into:

$$\tilde{V}_{agg}^{(\xi)}(\alpha) = \Delta_i e^{-jk\rho_{i_c^{(\xi)}l'^{(\xi)}}\cos(\alpha-\phi_{i^{(\xi)}l'^{(\xi)}})} \tag{12a}$$

$$\tilde{V}_{dgg}(\alpha) = \omega\mu/4Qe^{-jk\rho_{l j_c}\cos(\alpha-\phi_{lj})} \tag{12b}$$

which are the expressions for aggregation and disaggregation that can be found in the literature for two-dimensional problems [17, 18]. In the above equation, i_c, j_c are the centers of the cells i and j respectively, and Δ_i is the length of the i-th cell.

In our formulation, however, we have implemented a Galerkin scheme with triangular functions for both basis and test [19], combined for the first time with the FMM for two-dimensional problems. Therefore, we have evaluated directly equation (10a) by doing a simple numerical integration along the cells.

3.2. Building the MoM Matrix

The same strategy showed to reduce equation (7) into (8) can be followed for the rest of interactions in the problem (port to metal, metal to port or port to port). This can be done by simply adjusting the corresponding C expression in the aggregation/disaggregation operators, and by taking into account for the sign that appears in the image point. As shown in Section 2.1, this sign depends on the specific type of dyadic component involved in each case.

The FMM decomposition cannot be applied when the source and the observation points are very close to each other (in order to fulfill the addition theorem of the Hankel functions on which the FMM is based). Therefore, for a self-group and its nearest neighbours the interactions must be computed directly as in a normal MoM problem. As explained above, due to the nature of the Green's function employed in the external problem (spectral domain series), FMM cannot be applied in that case neither. Therefore, the corresponding calculations for that part will also be performed through a direct MoM process. Taking into account this final consideration for the definition of the nearest neighbours, the whole MoM matrix for this problem can be expressed as:

$$\boldsymbol{Z} = \boldsymbol{Z}_{\boldsymbol{NN}}^{\boldsymbol{tot}} + \boldsymbol{Z}_{\boldsymbol{FMM}}^{\boldsymbol{tot}} \tag{13}$$

In equation (13), $\boldsymbol{Z}_{\boldsymbol{NN}}^{\boldsymbol{tot}}$ is a sparse matrix containing all the interactions between nearest neighbours. This matrix must also include all the interactions between elements of the excitation port. If the groups are chosen so that the excitation port mesh is included in less

than three groups, this condition will be automatically fulfilled. On the other hand, the final $\boldsymbol{Z}_{\boldsymbol{FMM}}^{\boldsymbol{tot}}$ matrix is obtained as:

$$\begin{aligned} \boldsymbol{Z}_{\boldsymbol{FMM}}^{\boldsymbol{tot}} &= \boldsymbol{Z}_{\boldsymbol{FMM}}^{(\boldsymbol{s_o})} + \boldsymbol{Z}_{\boldsymbol{FMM}}^{(\boldsymbol{s_i})} \\ &= \bar{\boldsymbol{V}}_{\boldsymbol{dgg}} \cdot \bar{\boldsymbol{\alpha}}^{(\boldsymbol{s_o})} \cdot \bar{\boldsymbol{V}}_{\boldsymbol{agg}}^{(\boldsymbol{s_o})} + \bar{\boldsymbol{V}}_{\boldsymbol{dgg}} \cdot \bar{\boldsymbol{\alpha}}^{(\boldsymbol{s_i})} \cdot \bar{\boldsymbol{V}}_{\boldsymbol{agg}}^{(\boldsymbol{s_i})} \end{aligned} \tag{14}$$

where $\bar{\boldsymbol{V}}_{\boldsymbol{agg}}$, $\bar{\boldsymbol{\alpha}}$, and $\bar{\boldsymbol{V}}_{\boldsymbol{dgg}}$ are all sparse matrices that include the aggregation, translation and disaggregation operators showed above for all the interactions of the problem. As before, the superscripts (s_o) and (s_i) denote the cases of the original source and the spatial image respectively. Applying the decomposition in equation (13), the MoM linear system can be solved with an iterative solver, such as the biconjugate gradient, reducing the computational cost from $O(N^2)$ to $O(N^{1.5})$, without losing appreciable accuracy. This fact is demonstrated with the results that we present in the next section.

4. RESULTS

The software developed based on the technique presented finds applications in the analysis of many useful microwave circuits. First, we present two examples of inductive filters designed for satellite communications designed in [20]. The will show the results obtained employing both direct and FMM cases. Fig. 6 and Fig. 7 show the excellent agreement between the two approaches, and also with measurements included in [20]. The internal circuit is discretized with 346 segments for the 4-poles filter, and 408 for the 5-poles filter. Then, the coupling to the waveguide ports is modeled using 15 basis functions for both filters. On a PC computer with 2 GHz clock, the software takes 12.3 and 16.2 seconds per frequency point for the two cases respectively.

Another useful structure is a fourth order double rod filter composed of 10 circular posts, presented in [1], and shown in figure Fig. 8. In this case, 200 basis functions have been used for the internal problem and 24 for the ports. Again, good results between the direct and the FMM methods are observed. Also the agreement is very good with respect measurements presented in [1]. The software takes 11.7 seconds per frequency point on the same computer as before.

The next interesting structure that we investigate is the all inductive elliptic filters presented in [6]. Since all the cavities of the resonators have different widths, this structure can not be analyzed using a simple parallel plate Green's functions approach [5]. However, we can easily use the technique presented in this contribution, proving its versatility for practical microwave problems. As a first result, we present a filter with one dual mode cavity. The internal circuit is

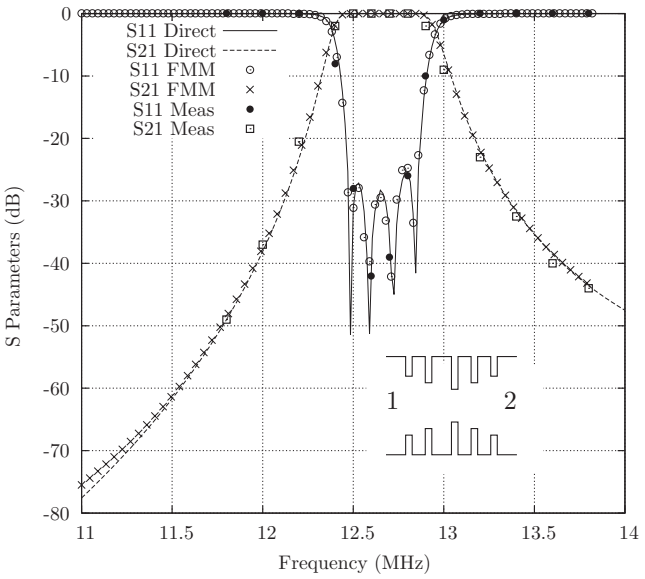

Figure 6. Scattering parameters of a filter with 4 cavities. Dimensions are shown in ref. [20].

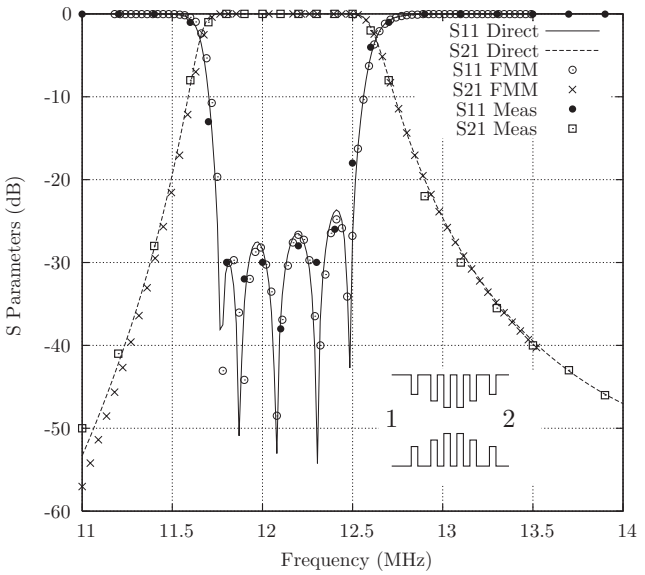

Figure 7. Scattering parameters of a filter with 5 cavities. Dimensions are shown in ref. [1].

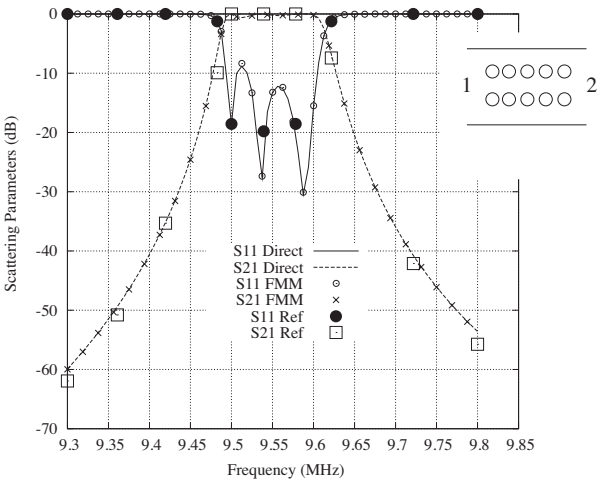

Figure 8. Scattering parameters of a filter with one dual mode cavity. Dimensions are shown in [6]-Fig. 4.

discretized with 175 segments, and then the coupling to the waveguide ports is modeled using 15 basis functions. Fig. 9 shows the results obtained for the scattering parameters of the filter. Measured results presented in [6], and simulations obtained with HFSS are also given, showing good agreement with our new technique. For this structure the software takes 5.8 seconds per frequency point.

A more complex filter with two dual mode cavities exhibiting elliptic response was also designed in [6]. Fig. 10 shows the measured and simulated results calculated with the new approach. Reference results obtained with HFSS are also included for validation. Again, good agreement with the new technique can be observed. In this case a total of 241 basis functions were used for the discretization of the internal circuit topology, and 15 basis functions for the ports. The software takes 9.2 seconds per frequency point for this structure.

The multiport nature of the tool developed can be best discussed with the analysis of a T-junction, where three ports must be treated at the same time. In this case we have selected a T-junction compensated by a cylindrical post, presented in [8]. Fig. 11 presents measured and simulated results for the reflection coefficient at the common port. Reference results obtained with HFSS are again included for validation. We can see good agreement with the simulation results obtained with our new technique, for both direct and FMM cases. For this analysis, 129 basis functions are used for the circuit and 20 for the ports. The software takes 5.4 seconds per frequency point. In all above examples,

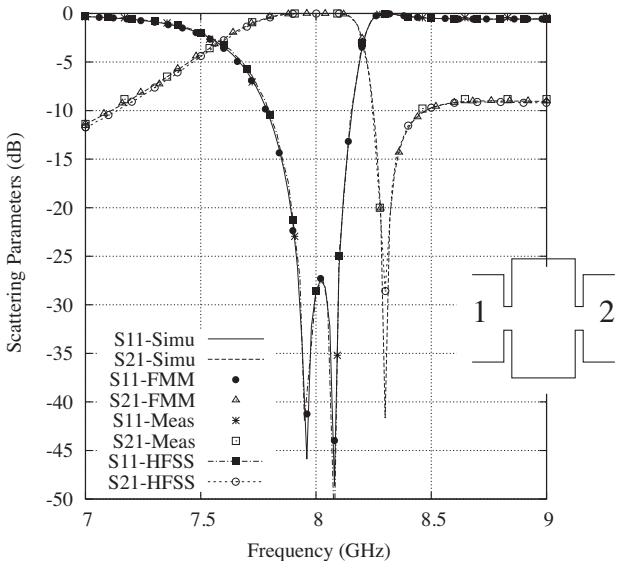

Figure 9. Scattering parameters of a filter with two dual mode cavities. Dimensions are shown in [6]-Fig. 6.

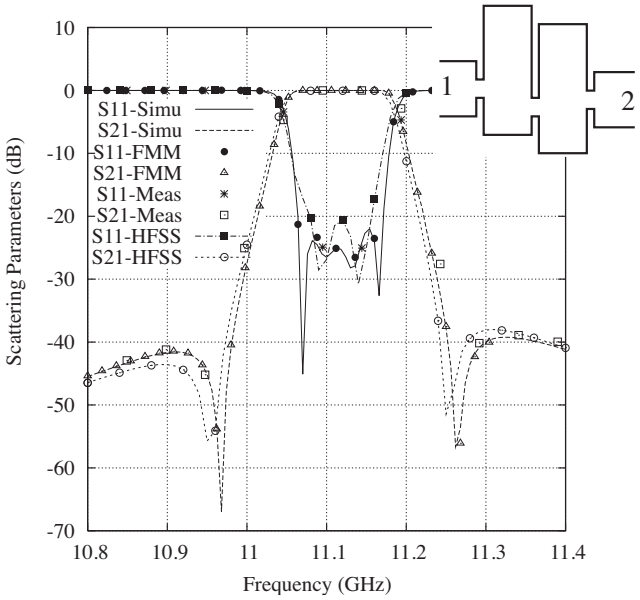

Figure 10. Reflection coefficient of the common port for the T-junction presented in [8]-Fig. 2.

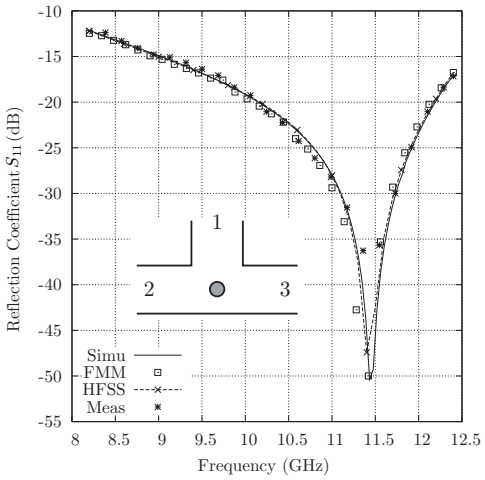

Figure 11. Reflection coefficient of the common port for the T-junction presented in [8]-Fig. 2.

the ports are all oriented either horizontally or vertically. In order to validate the port treatment for different orientations, we have further analyzed an inductive bend with different bend-angles, as presented in [8]. Fig. 12 shows the reflection coefficient when the angle of the bend is varied from 90° to 150°. Results reported in [8] and results obtained with HFSS are given for comparison. Again good agreement is obtained for angle bends smaller than 135°. When the angle is 150°, our results agree better with those obtained using the Finite Elements technique (HFSS). Again, it can be seen that our FMM approach works perfectly with ports with arbitrary orientations, without lost of accuracy with respect to the direct MoM solution. For the analysis of this structure a total of 83 basis functions were used for the circuit and 15 for the ports. The software takes 1.9 seconds per frequency point.

In order to show the advantages of the usage of the FMM approach, let us consider the examples of the double-rod filter in Fig. 7, and of the T junction in Fig. 10. For the first case, if the number of basis functions is increased up to 680, the FMM allows to reduce the CPU time per frequency point in 22.2%. For the T-junction case, the FMM allows to save 35.6% of memory for data storage, and up to 35.7% of CPU time per frequency point when using 1010 basis functions. These simple examples show the interest in employing the FMM formulation derived in this paper, when the number of unknowns increases in a particular application.

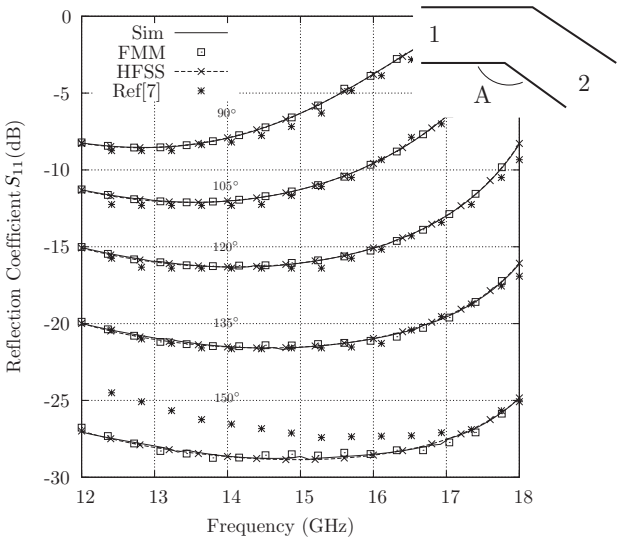

Figure 12. Reflection coefficient for bends with varying angle α from 90° to 150°. Dimensions are shown in [8]-Fig. 3a.

5. CONCLUSIONS

In this paper an alternative surface integral equation formulation is proposed for the analysis of complex inductive waveguide microwave devices. The technique uses the extinction theorem to separate the internal circuit problem from the input/output ports. A formulation has been presented to express the Green's functions of the internal circuit problem with respect to an arbitrarily oriented ground plane. For the external port problem the infinite parallel plate waveguide Green's functions of magnetic type are used. Unlike traditional approaches, the Green's functions are obtained in the space domain by using series acceleration techniques. Besides, the FMM decomposition technique has been successfully applied in order to reduce the computational cost for large problems. Results are presented for several practical microwave devices, including bandpass filters with elliptic transfer functions, inductive bends and T-junctions. Comparisons with measured data confirm the accuracy and the computational efficiency of the technique presented. The application of the FMM allows to save both memory and CPU time, when solving problems with large number of unknowns.

REFERENCES

1. Yin, S., T. Valilyeva, and P. Pramanick, "Use of three-dimensional field simulators in the synthesis of waveguide round rod bandpass filters," *Int J Microwave and Millimeter Wave Computer Aided Engineering*, Vol. 8, 484–497, August 1998.
2. Reiter, J. M. and F. Arndt, "Rigorous analysis of arbitrarily shaped H- and E-plane discontinuities in rectangular waveguides by a full-wave boundary contour mode-matching method," *IEEE Transactions on Microwave Theory and Techniques*, Vol. 43, No. 4, 796–801, April 1995.
3. Rozzi, T., F. Moglie, A. Morini, W. Gulloch, and M. Politi, "Accurate full-band equivalent circuits of inductive posts in rectangular waveguide," *IEEE Transactions on Microwave Theory and Techniques*, Vol. 40, No. 5, 1000–1009, May 1992.
4. Guglielmi, M., G. Gheri, M. Calamia, and G. Pelosi, "Rigorous multimode network numerical representation of inductive step," *IEEE Transactions on Microwave Theory and Techniques*, Vol. 42, No. 2, 317–326, February 1994.
5. Auda , H. and R. F. Harrington, "Inductive posts and diaphragms of arbitrary shape and number in a rectangular waveguide," *IEEE Transactions on Microwave Theory and Techniques*, Vol. 32, No. 6, 606–613, June 1984.
6. Guglielmi, M., P. Jarry, E. Kerherve, O. Roquebrun, and D. Schmitt, "A new family of all-inductive dual-mode filters," *IEEE Transactions on Microwave Theory and Techniques*, Vol. 49, No. 10, 1764–1769, October 2001.
7. Esteban, H., S. Cogollos, V. E. Boria, A. A. San Blas, and M. Ferrando, "A new hybrid mode-matching/numerical method for the analysis of arbitrarily shaped inductive obstacles and discontinuities in rectangular waveguides," *IEEE Transactions on Microwave Theory and Techniques*, Vol. 50, No. 4, 1219–1224, April 2002.
8. Reiter, J. M. and F. Arndt, "Rigorous analysis of arbitrarily shaped H- and E-plane discontinuities in rectangular waveguides by a full wave boundary contour mode matching method," *IEEE Transactions on Microwave Theory and Techniques*, Vol. 43, No. 4, 796–801, April 1995.
9. Catina, V., F. Arndt, and J. Brandt, "Hybrid surface integral equation/mode-matching method for the analysis of dielectric loaded waveguide filters of arbitrary shape," *IEEE Transactions on Microwave Theory and Techniques*, Vol. 53, No. 11, 3562–3567,

November 2005.

10. Leviatan, Y. and G. S. Sheaffer, "Analysis of inductive dielectric posts in rectangular waveguide," *IEEE Transactions on Microwave Theory and Techniques*, Vol. 35, No. 1, 48–59, January 1987.
11. Li, P. G., A. T. Adams, Y. Leviatan, and J. Perini, "Multiple post inductive obstacles in rectangular waveguide," *IEEE Transactions on Microwave Theory and Techniques*, Vol. 32, No. 4, 365–373, April 1984.
12. Geng, N., A. Sullivans, and L. Carin, "Multilevel fast multipole algorithm for scattering from conducting targets above or embeded in lossy half space," *IEEE Microwave and Wireless Components Letters*, Vol. 38, No. 4, 115–125, July 2000.
13. Zhao, Z. Q., L. Li, J. Smith, and L. Carin, "Analysis of scattering from very large three dimensional rough surfaces using MLFMM and rat-based analysis," *IEEE Antennas and Propagation Magazine*, Vol. 47, No. 3, 20–30, June 2005.
14. Melcon, A. A. and J. R. Mosig, "A novel spatial images technique for the analysis of cavity backed antennas," *ACES, Applied Computational Electromagnetics Society*, Vol. 14, No. 3, March 1999.
15. Melcon, A. A. and J. R. Mosig, "Two techniques for the efficient numerical calculation of the Green's functions for planar shielded circuits and antennas," *IEEE Transactions on Microwave Theory and Techniques*, Vol. 48, No. 9, 1492–1504, September 2000.
16. He, J., A. Sullivan, and L. Carin, "Multi-level fast multipole algorithm for general dielectric targets in the presence of a lossy half space," *Radio Science*, Vol. 36, 1271–1285, November–December 2001.
17. Chew, W. C., J.-M. Jin, E. Michielssen, and J. Song, *Fast and Efficient Algorithms in Computational Electromagnetics*, Chap. 2, Artech House, 2001.
18. Chew, W. C. and C. C. Lu, "Fast algorithm for solving hybrid integral equation," *IEE Proceedings-H*, Vol. 140, 455–459, December 1993.
19. Rao, S. M., D. R. Wilton, and A. W. Glisson, "Electromagnetic scattering by surfaces of arbitrarily shape," *IEEE Transactions on Antennas and Propagation*, Vol. 30, No. 5, 409–418, May 1982.
20. Guglielmi, M., G. Gheri, and A. A. Melcon, *CAD of Tunnning-Less Band-Pass Filters*, 1624, European Space Agency, ESA-ESTEC, Noordwijk, The Netherlands, July 1991.